Supporting Information

Experimental section

The encapsulated guest material within the coaxial carbon nanocables (CNCs)

The open-ended CNCs were separately sealed with sublimed sulfur, phenyl-C_{61}-butyric acid methyl ester solution or polyvinylidene fluoride in a Pyrex flask, followed by degassing to a vacuum state. The sealed flasks were heated at 80, 60 and 175°C for sublimed sulfur, phenyl-C_{61}-butyric acid methyl ester solution and polyvinylidene fluoride for 2 d, respectively. The resulting mixtures were accordingly washed with carbon disulfide, chlorobenzene and dimethyl formamide to remove the materials at the outer surfaces of CNCs.

Characterization

The electrochemical performance was evaluated in coin cells (CR2032) with the CNC slices as a working electrode and lithium foil as the counter/reference electrode. The weights of CNC arrays were in the range of 0.1–0.5 mg, depending on the growth time. The CNC arrays were cut into slices, and all the CNC slices were collected and served as active materials. A poly (vinylidene fluoride) solution in N-methyl-2-pyrrolidone (weight concentration of 0.5%) was drop-coated onto the CNC slice after it was paved on the button inside. The electrolyte was composed of 1.0 M $LiPF_6$ in a solvent mixture of ethylene carbonate, diethyl carbonate and dimethyl carbonate ethylene with weight ratios of 1/1/1. The measurements were performed at an Arbin electrochemical station (MSTAT-5 V/10 mA/16Ch) at a voltage range of 0.005 to 3 V *versus* Li/Li^+ for charge-discharge and cyclic voltammetry. The current density was calculated as the current value divided by the mass of electrode. Here, the mass of non-doped and N-doped CNC slices were 0.15 and 0.5 mg, respectively. The current values were similar to the previous reports.[1-3]

To clarify whether the battery reactions were lithium ion adsorbing or charge-transfer lithiation reaction, symmetrical capacitor was assembled by using the same CNC slices as two electrodes with lithium ion electrolyte (Fig. S15). The specific capacity was calculated as only 16 F/g. Low capacity illustrated the battery reaction of CNC slices was a lithium insertion and extraction process.

The structures were characterized by scanning electron microscopy (SEM, Hitachi FE-SEM S-4800) and transmission electron microscopy (TEM, JEM-2100F). Energy-

filtered transmission electron microscopy was conducted by electron energy loss spectroscopy (Gatan GIF-Tridiem). X-ray diffraction patterns and Raman spectra were recorded from an X-ray single crystal diffractometer (Bruker SMART APEX (II)-CCD) and Laser-Raman microspectroscopy (Renishaw in Via Reflex, 633 nm), respectively.

Notes and References

[1] W. Shin, H. Jeong, B. Kim, J. Kang, J. Choi, *Nano Lett.* **2012**, 12, 2283.

[2] Z. Pan, J. Ren, G. Guan, X. Fang, B. Wang, S.-G. Doo, I. H. Son, X. Huang, H. Peng, *Adv. Energ. Mater.* **2016**, 6, 1600271.

[3] W. Ren, D. Li, H. Liu, R. Mi, Y. Zhang, L. Dong, *Electrochim. Acta* **2013**, 105, 75.

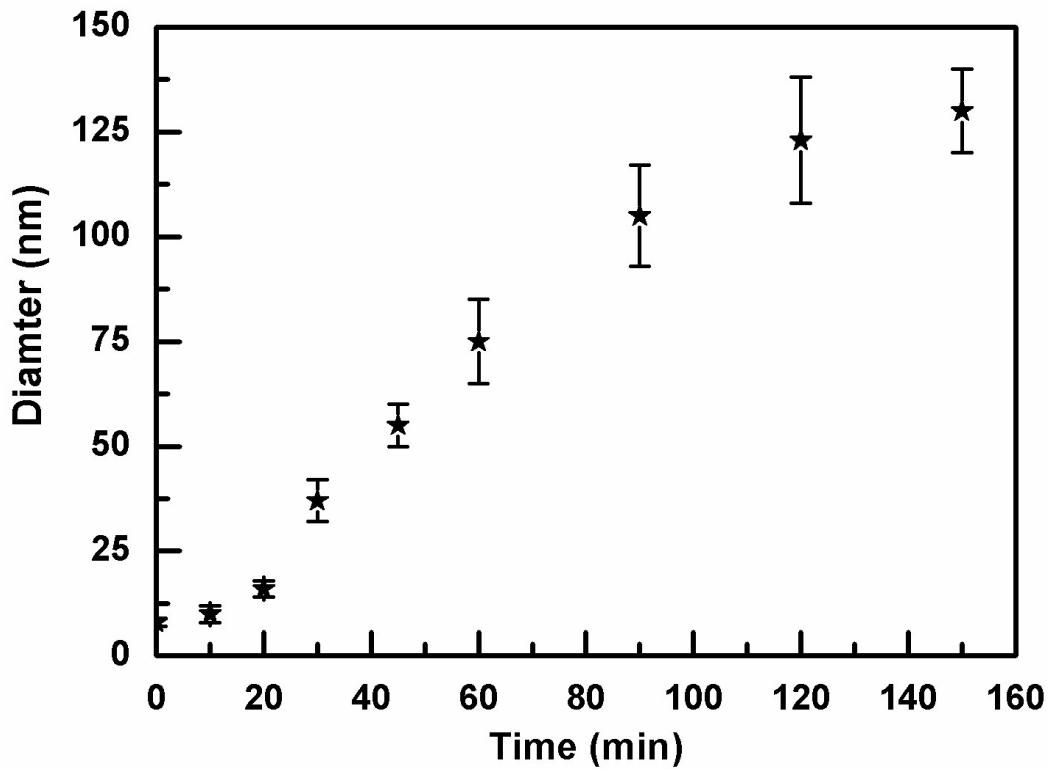

Fig. S1. Dependence of CNC diameter on re-growth time.

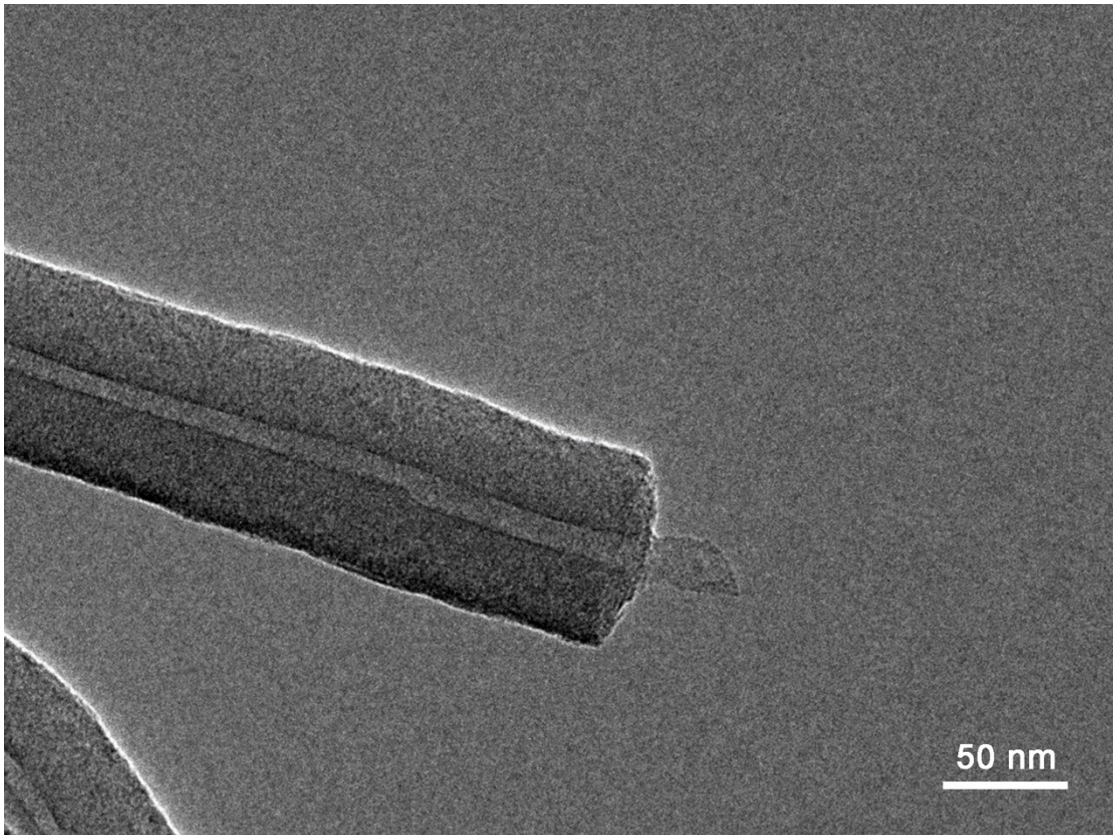

Fig. S2. High-resolution transmission electron microscopy (TEM) images of newly grown graphene layers concentrically wrapped around the pristine carbon nanotubes.

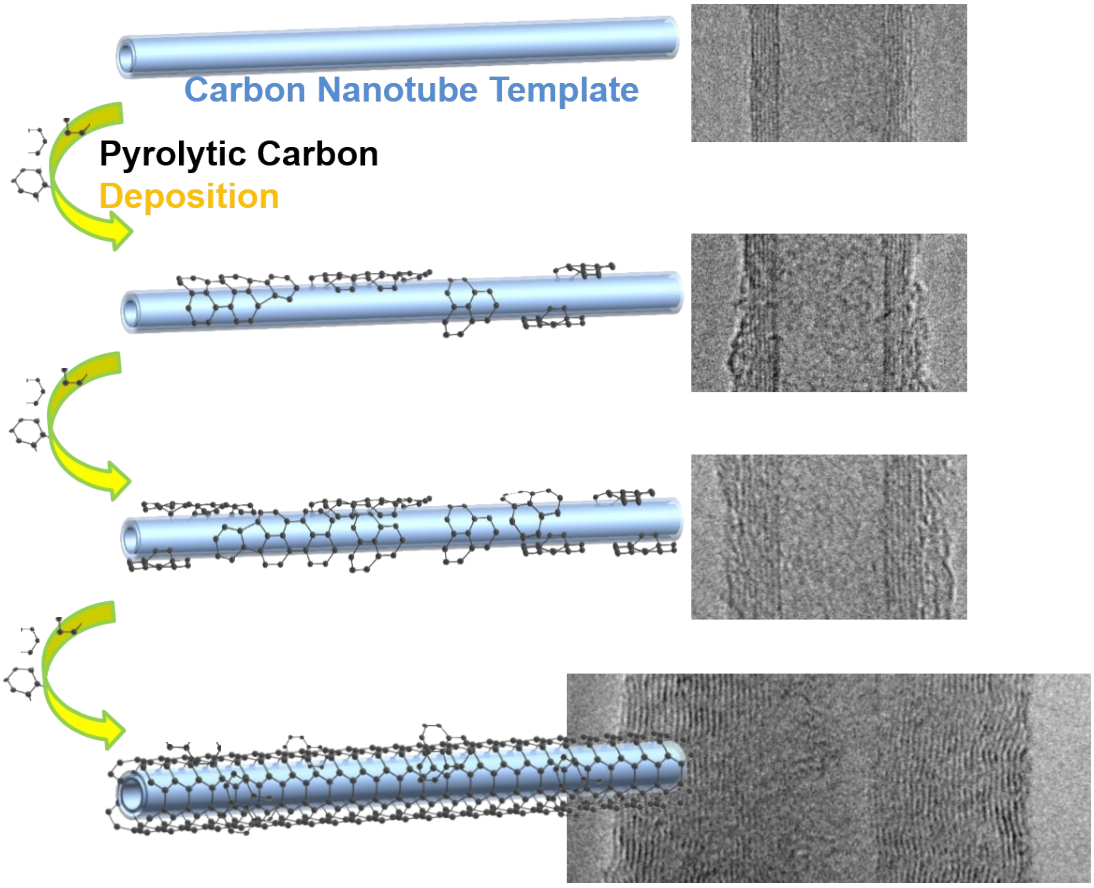

Fig. S3. Schematic illustration to the formation of the CNC with related high-resolution TEM images.

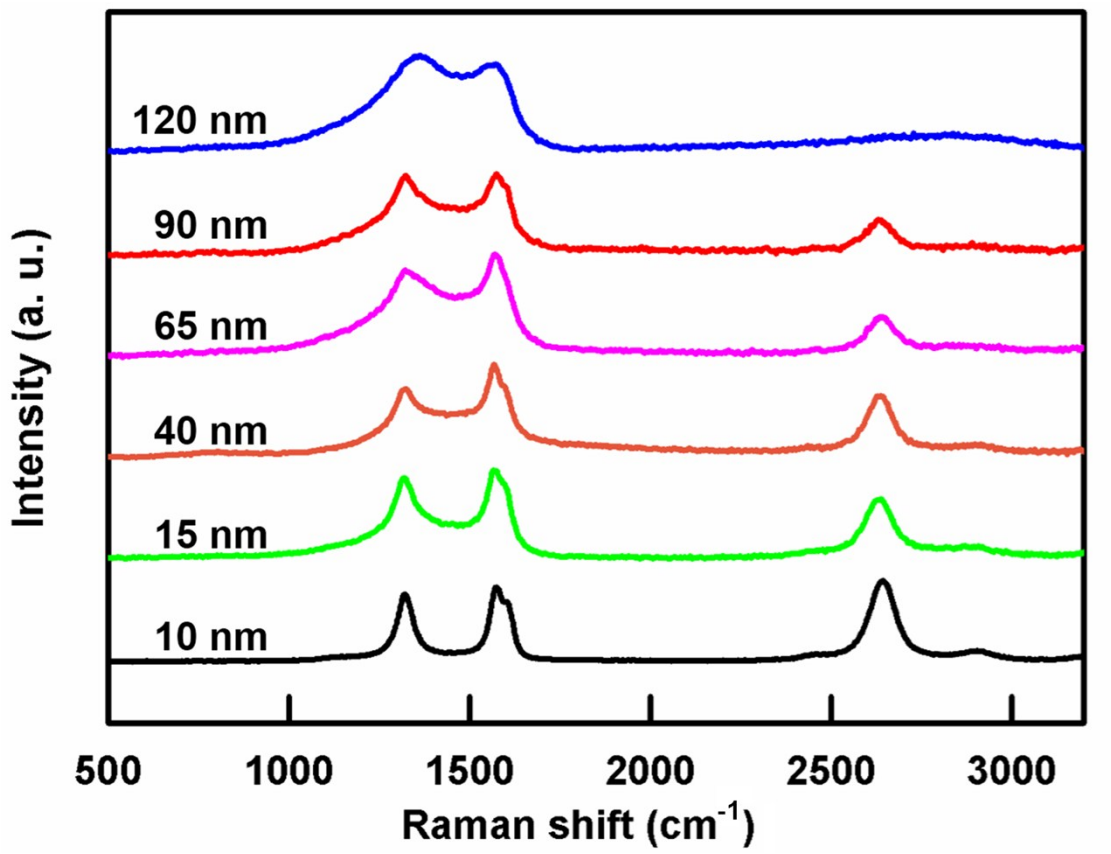

Fig. S4. Raman spectra of CNCs with increasing diameters from 10 to 120 nm.

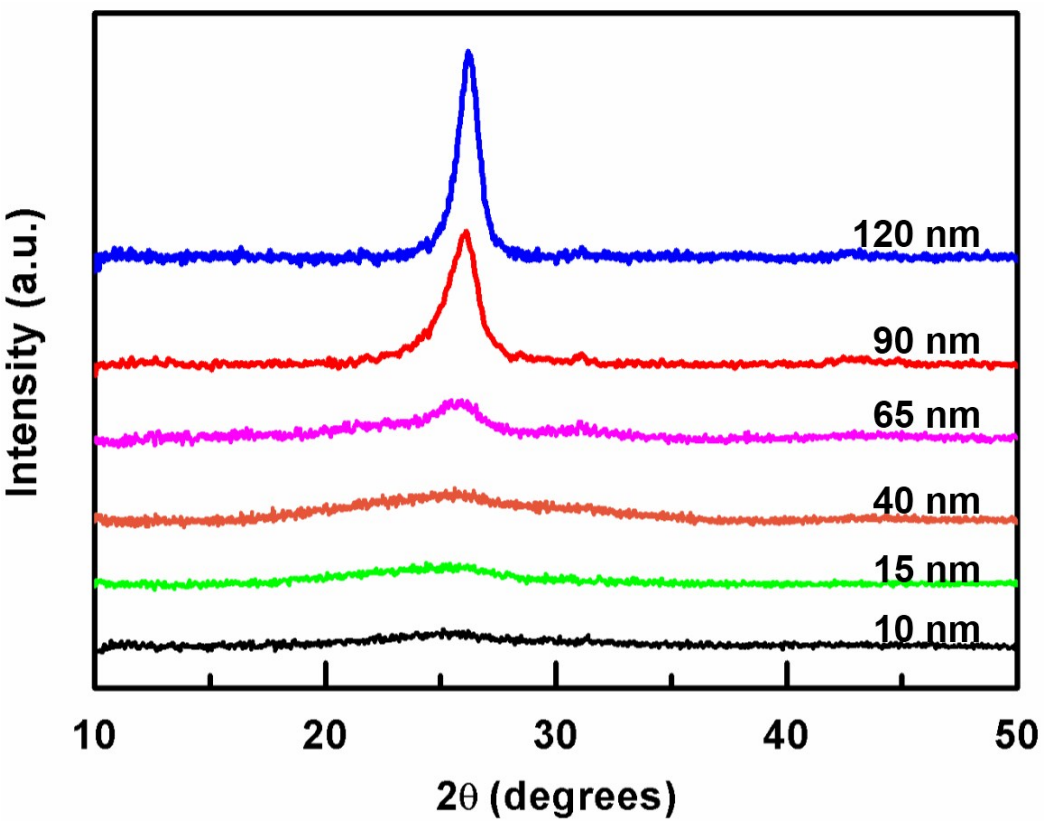

Fig. S5. X-ray diffraction patterns of CNCs with increasing diameters from 10 to 120 nm.

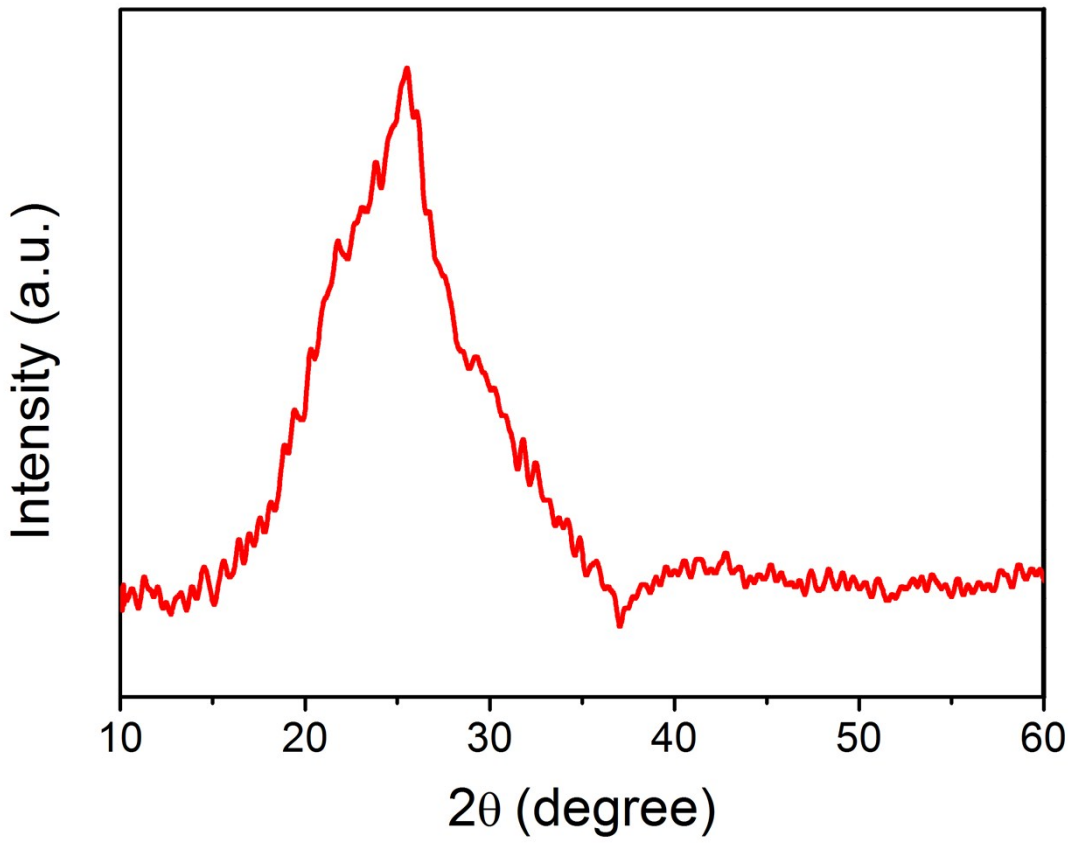

Fig. S6. X-ray diffraction patterns of pristine CNT arrays.

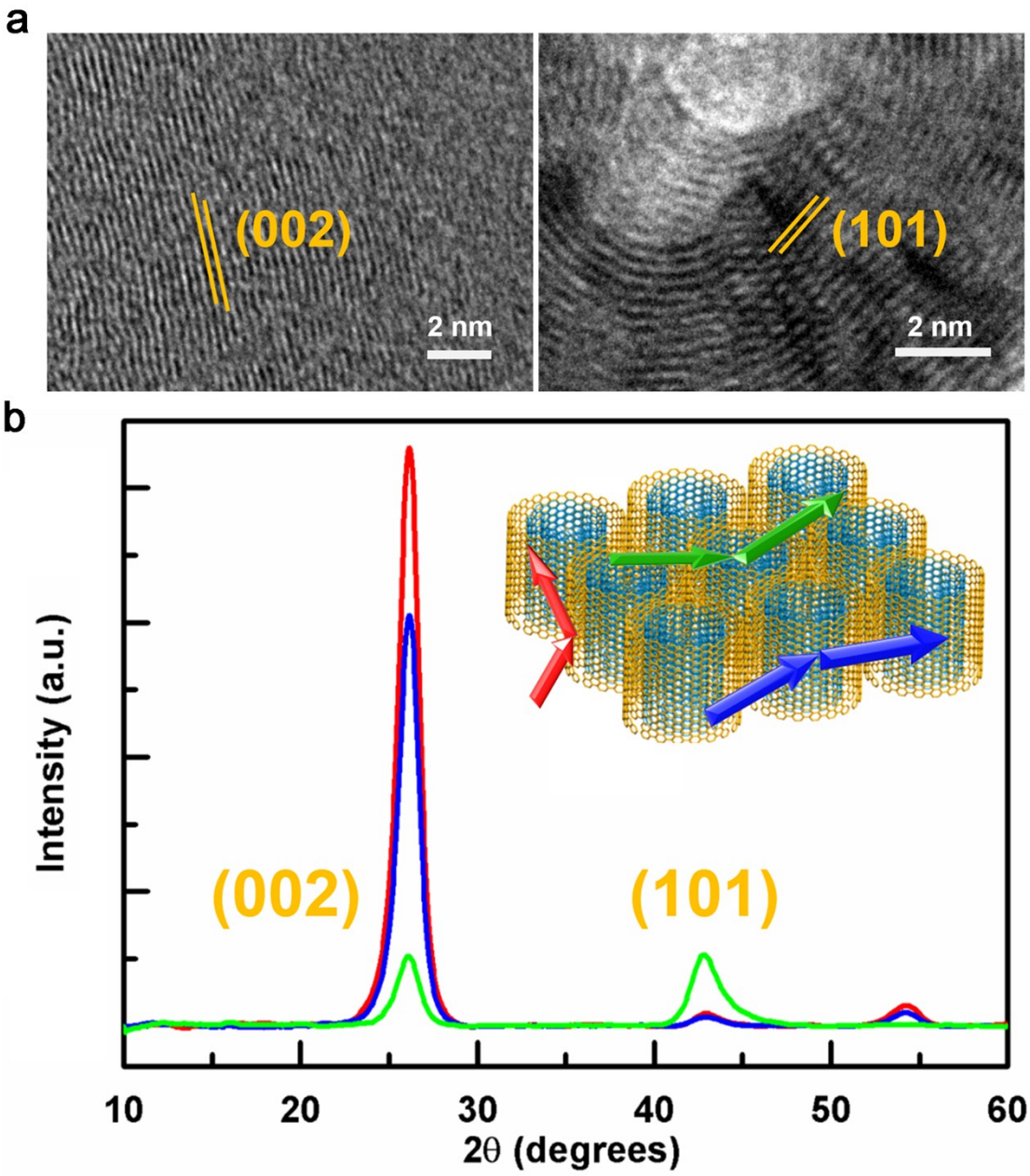

Fig. S7. Anisotropy of the highly aligned CNC array. a) High-resolution TEM images of CNCs with different lattice planes. b) X-ray diffraction patterns recorded from different directions labelled at the inserted scheme.

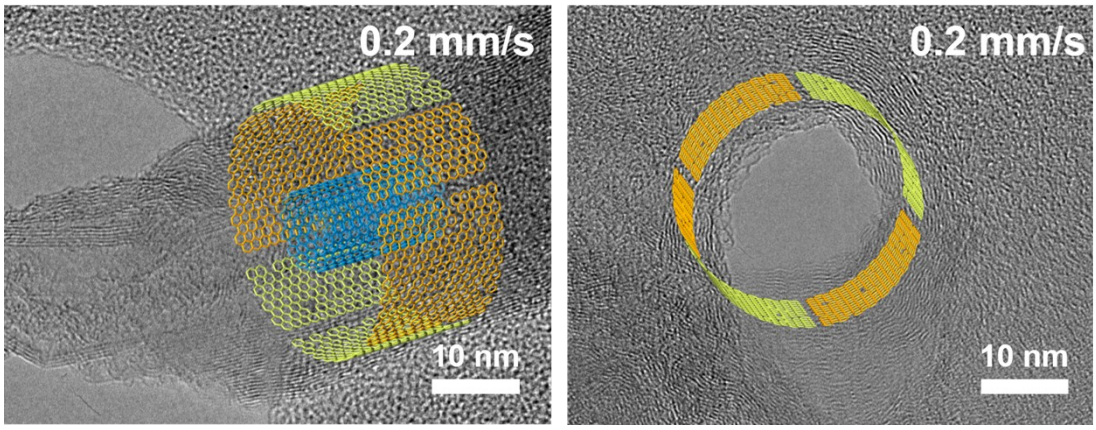

Fig. S8. High-resolution TEM images of CNCs after cutting with a feeding speed of 0.2 mm/s by side (left) and top (right) views.

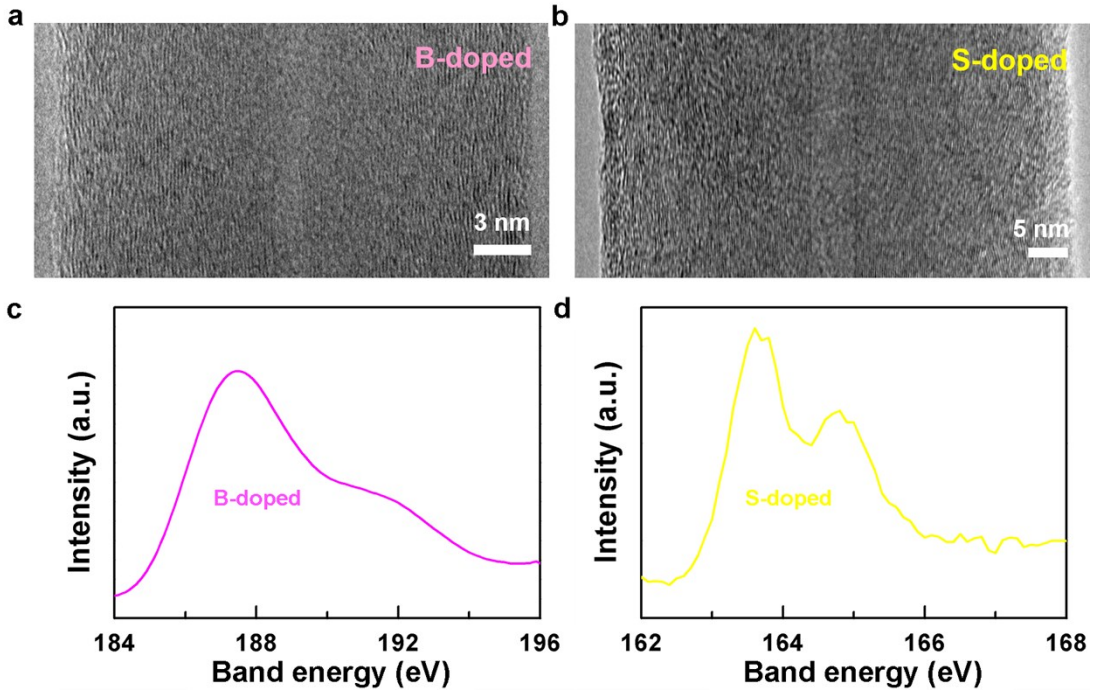

Fig. S9. a, b) High-resolution TEM images of CNCs with outer sheaths doped with B and S, respectively. c, d) X-ray photoelectron spectroscopy characterizations of the highly aligned B-doped and S-doped CNC arrays, respectively.

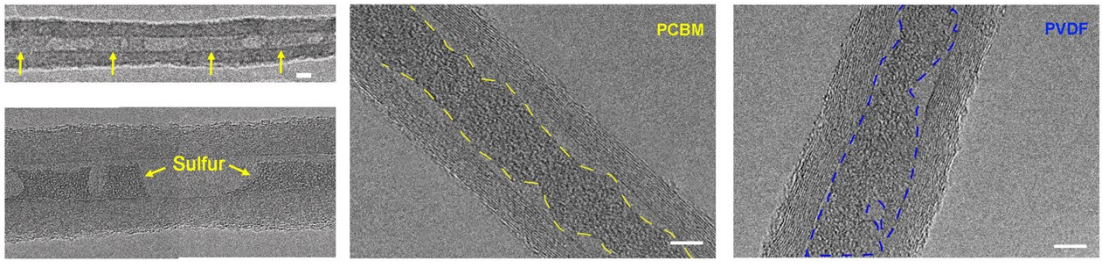

Fig. S10. High-resolution TEM image of an open-end CNC filled with sulfur, phenyl-C_{61}-butyric acid methyl ester and polyvinylidene difluoride. Scale bar: 5 nm.

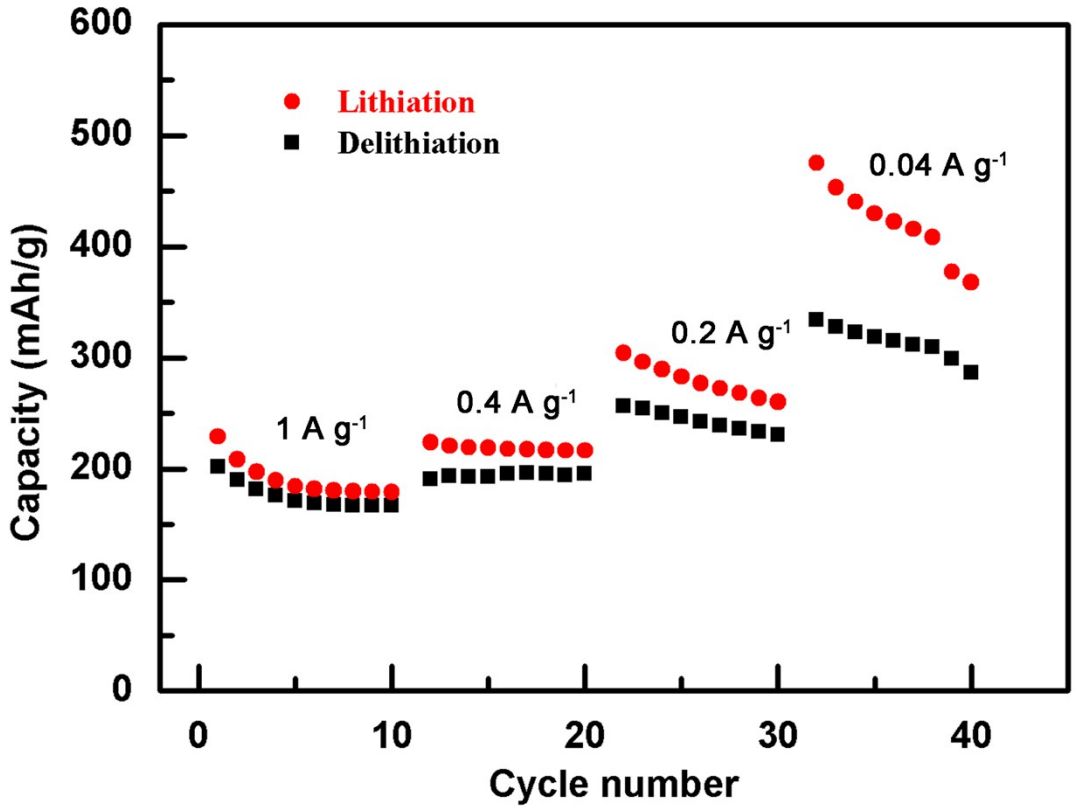

Fig. S11. Li-ion battery rate performance of CNC arrays before cutting.

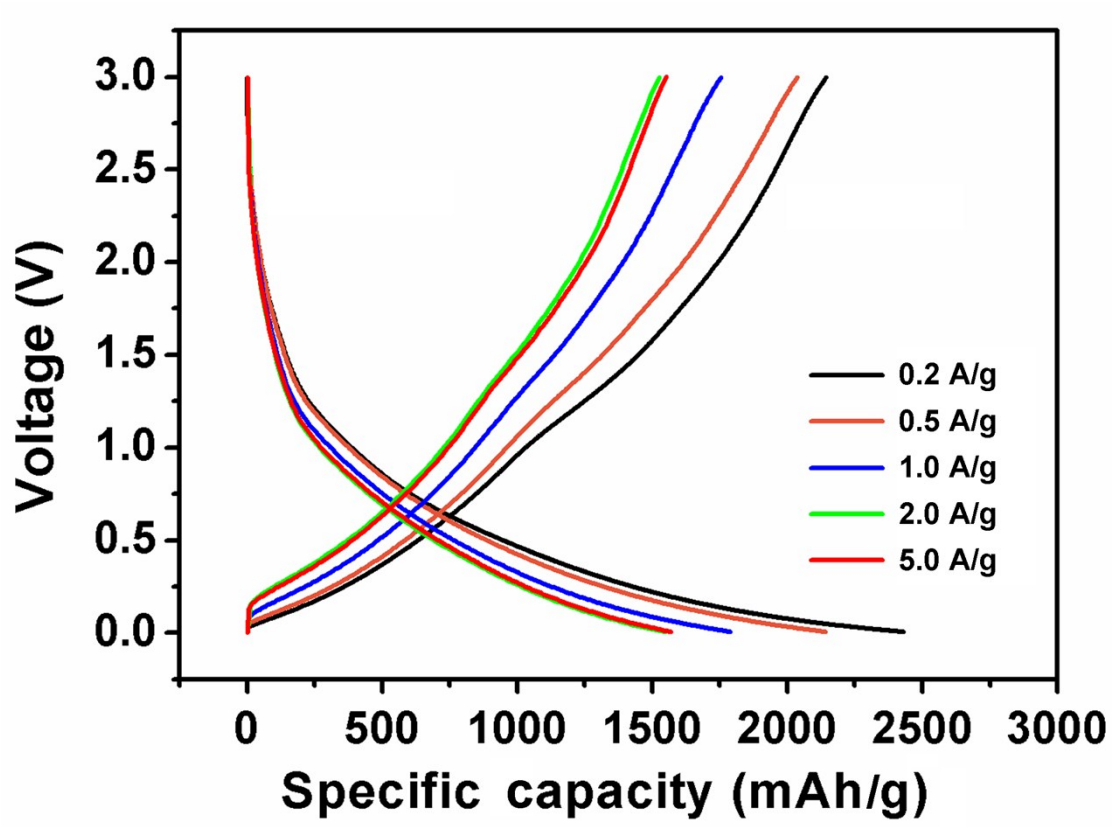

Fig. S12. Charging and discharging curves of N-doped CNC slices at rates of 0.2, 0.5, 1, 2 and 5 A/g.

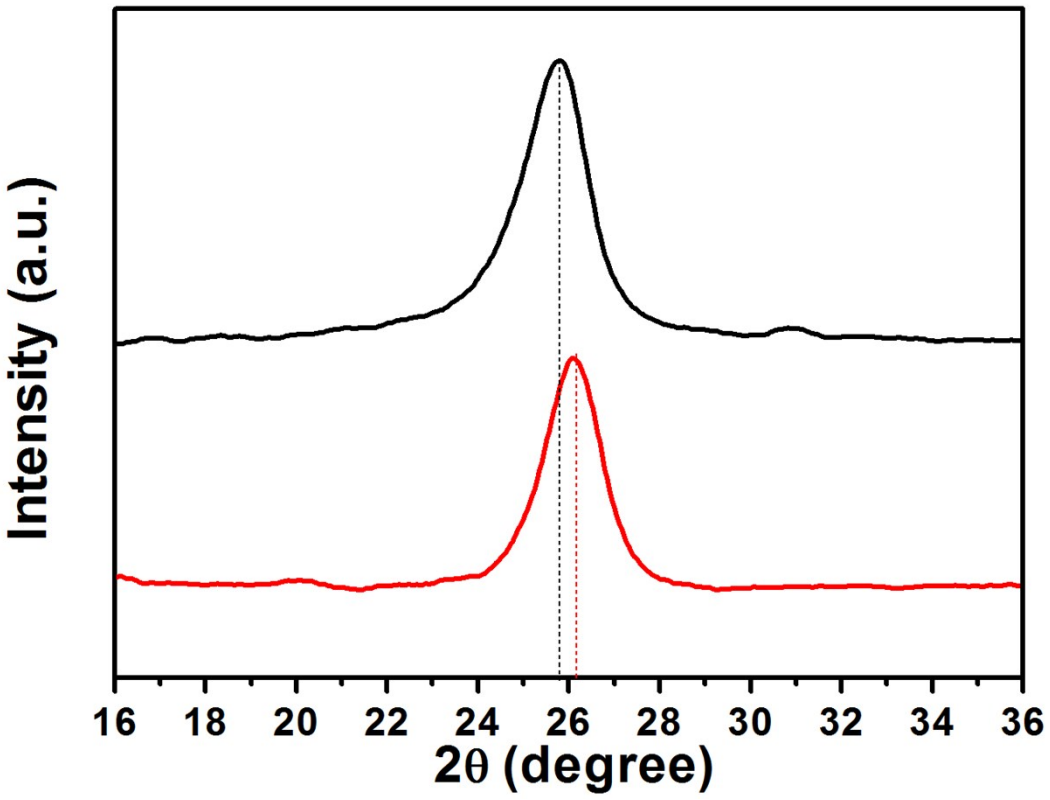

Fig. S13. X-ray diffraction patterns of CNCs before (red line) and after (black line) the first cycle of charging-discharging process.

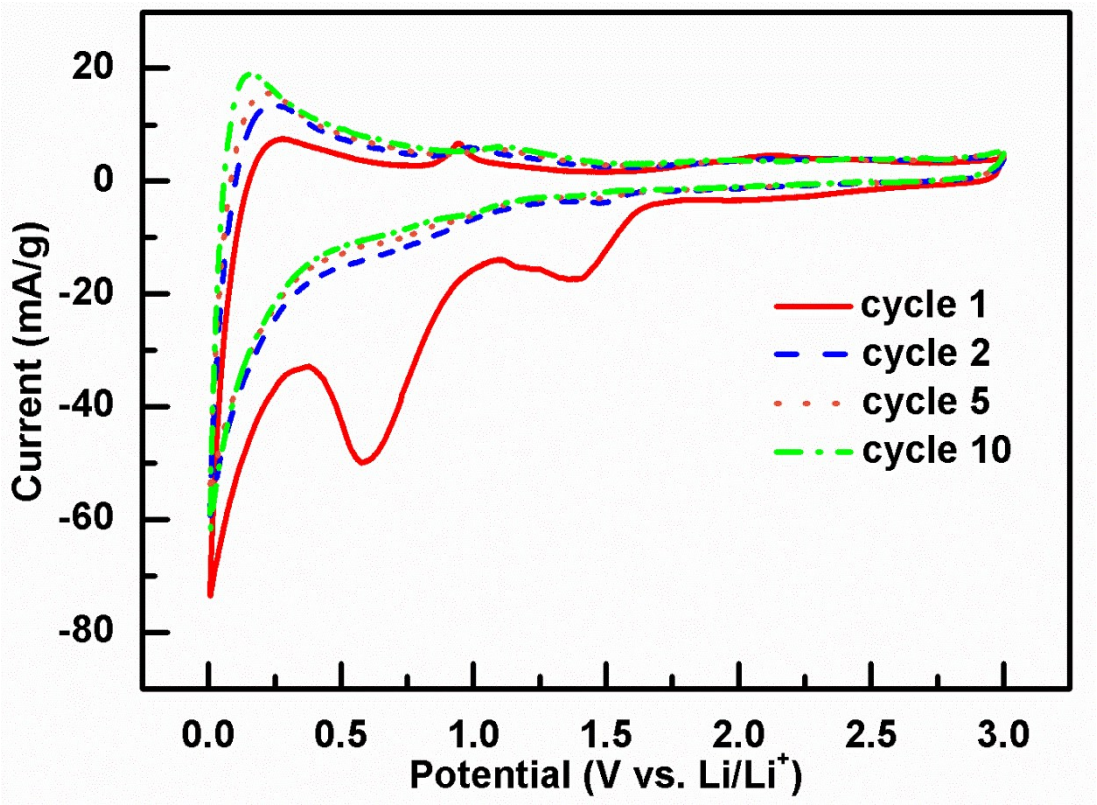

Fig. S14. Cyclic voltammograms of the highly aligned non-doped CNC slices at a scan rate of 0.2 mV/s.

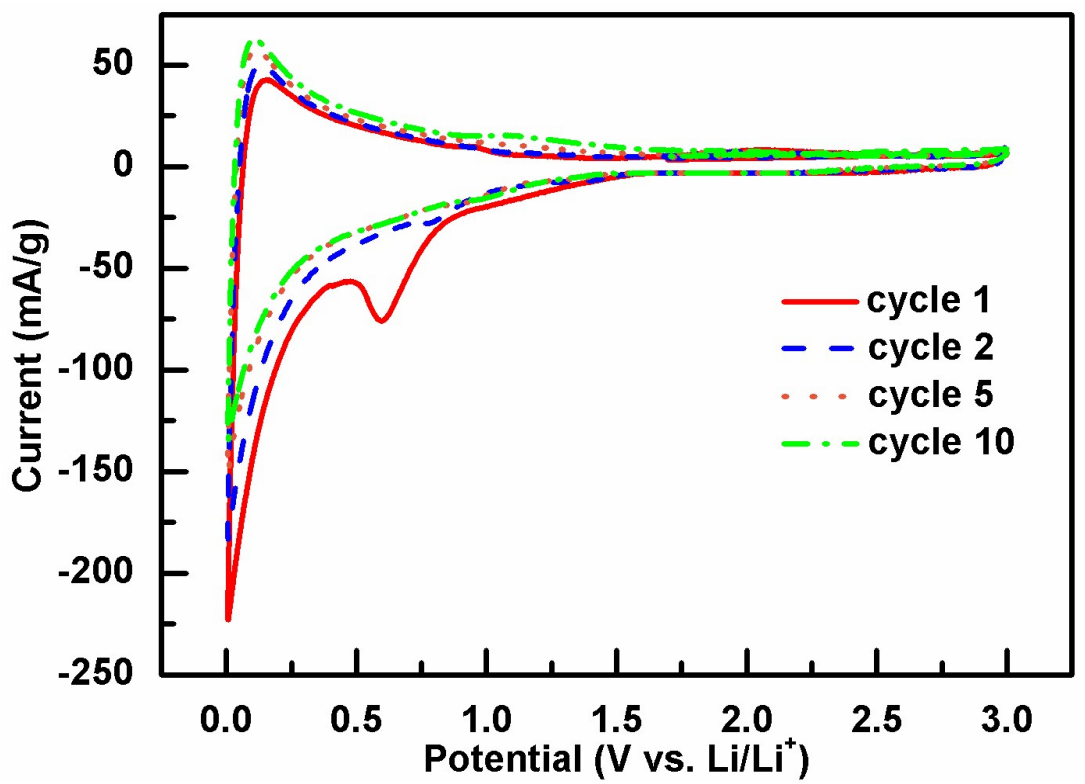

Fig. S15. Cyclic voltammograms of the highly aligned N-doped CNC slices at a scan rate of 0.2 mV/s.

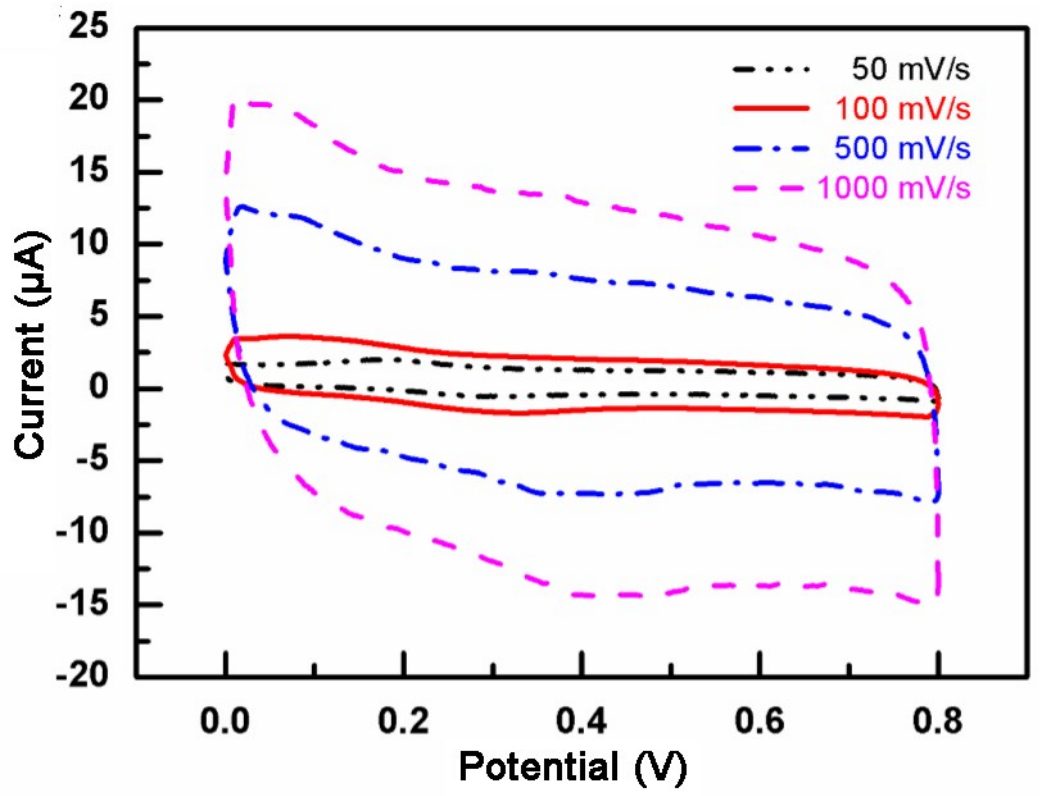

Fig. S16. CV curves of a symmetrical capacitor assembled from the same CNC slices as two electrodes with increasing scan rates.